Dispersion coefficients for the interactions of the alkali-metal and alkaline-earth-metal ions and inert-gas atoms with a graphene layer

Kiranpreet Kaur and Bindiya Arora*
Department of Physics, Guru Nanak Dev University, Amritsar, Punjab 143005, India

B. K. Sahoo†
Theoretical Physics Division, Physical Research Laboratory, Navrangpura, Ahmedabad 380009, India
(Received 18 June 2015; published 8 September 2015)

Largely motivated by a number of applications, the van der Waals dispersion coefficients C_3 of the alkali-metal ions Li^+, Na^+, K^+, and Rb^+, the alkaline-earth-metal ions Ca^+, Sr^+, Ba^+, and Ra^+, and the inert-gas atoms He, Ne, Ar, and Kr with a graphene layer are determined precisely within the framework of the Dirac model. For these calculations, we evaluate the dynamic polarizabilities of the above atomic systems very accurately by evaluating the transition matrix elements employing relativistic many-body methods and using the experimental values of the excitation energies. The dispersion coefficients are given as functions of the separation distance of an atomic system from the graphene layer and the ambiance temperature during the interactions. For easy extraction of these coefficients, we give a logistic fit to the functional forms of the dispersion coefficients in terms of the separation distances at room temperature.

DOI: 10.1103/PhysRevA.92.032704 PACS number(s): 34.20.Cf, 73.22.Pr, 78.67.−n, 12.20.Ds

I. INTRODUCTION

Since carbon nanostructures are highly sensitive to their thermal, mechanical, and electrical properties, they are extensively used for both scientific and industrial applications. Hence, their studies are of great importance in the scientific community [1–3]. Some of the prominent applications include their utility in nanotechnology, biochemical sensors, optics, electronics, new composite materials [4–6], ion storage, nanoelectromechanical systems and ion channeling in carbon nanotubes (CNTs), secured wireless connections, and efficient communication devices [7,8]. Among various carbon nanostructures, graphene, a one-atom-thick layer of carbon with remarkable properties, has been recently given considerable attention. It is of much significance in the areas of development of sensor technologies [8,9], encapsulation of drugs [8,10,11], nanofiltration membranes, regulating carbon dioxide for tackling climate change, etc. Moreover, it has been observed that the interaction of graphene with various species such as atoms, molecules, or ions can change its electronic and magnetic properties [12,13] and it is being studied extensively in the context of the phenomenon of quantum reflection. Interactions of the alkali-metal atoms with a graphene layer have been recently investigated in Refs. [14,15] and with a single-walled CNT in Ref. [16]. Since these interactions are extremely weak, it is immensely difficult to measure them precisely using any experimental technique. Instead, sophisticated theoretical studies are carried out to find them more reliably. A number of calculations have been reported using a wide variety of many-body methods, such as density-functional theories [17–21] and lower-order many-body methods [22], to study the nature of the interaction of the carbon nanostructures with various materials such as ions, atoms, and molecules [14,23–25]. For example, the interactions of a graphene layer with metal plates [26–28], with the H [29], Na, Rb, and Cs [14,29] atoms, and with the H_2 molecule [29] have been investigated in the Lifshitz theory framework. Due to the significance of studying the atomic system and graphene interactions accurately, it would be useful to explore the behavior of these interactions for other atomic systems such as the presently considered alkali-metal ions, alkaline-earth-metal ions, and inert-gas atoms with a graphene layer. The primary interest in choosing these particular atomic systems is for their applications to modern technology. For instance, the interaction of the lithium ion Li^+ with graphene has applications in enhancing lithium storage capacity in lithium ion cells [30,31] and improving the performance of rechargeable lithium ion batteries [8,32]. Similarly, the interaction of the alkaline-earth-metal ions with the carbon nanostructures has potential applications in heterogeneous catalysis, biosensing [8], hydrogen storage [33–35] for powering green vehicles, molecular sieving, water desalination, etc. In the Lifshitz theory, these interactions can be explained using two models: the hydrodynamic model [36–38] and the Dirac model [39]. Of these two models the Dirac model is more adequate [40] since it considers the quasiparticle fermion excitations in the graphene as massless Dirac fermions moving with the Fermi velocity. In fact, recent studies have demonstrated that the Dirac model is in better agreement with the experimental data on measuring the Casimir force between an Au sphere and a graphene-coated substrate than the hydrodynamic model [41]. Accuracy in the determination of the atom-wall interactions also depends on the accuracy of the dynamic polarizabilities of the atomic systems that appears in the formulas of the Lifshitz theory. For instance, the role of using accurate values of the dynamic polarizabilities of the alkali-metal atoms to describe interactions of these atoms with a graphene layer in both the hydrodynamic and Dirac models at zero temperature was emphasized in Ref. [16]. In this work we intend to calculate the dispersion coefficients of the

*arorabindiya@gmail.com
†bijaya@prl.res.in

alkali-metal ions (Li^+, Na^+, K^+, and Rb^+), alkaline-earth-metal ions (Ca^+, Sr^+, Ba^+, and Ra^+), and inert-gas atoms (He, Ne, Ar, Kr, and Xe) with a graphene layer at room temperature using accurately estimated polarizability values.

II. THEORY OF DISPERSION COEFFICIENT

The general expression of the van der Waals and Casimir-Polder energies in terms of the dispersion C_3 coefficient for an atomic system interacting with a graphene layer is expressed as [29]

$$E(a) = -\frac{C_3}{a^3}, \tag{1}$$

where a is the separation distance between the atom or ion from the graphene layer. The explicit expressions for the C_3 coefficients at zero temperature and nonzero temperature (in Kelvin), in terms of the reflection coefficients $r_{\rm TM}$ and $r_{\rm TE}$, are given by [14,15,42]

$$C_3(a) = -\frac{1}{16\pi}\int_0^\infty d\xi\,\alpha(\iota\xi)\int_{2a\xi\alpha_{\rm FS}}^\infty dy\,e^{-y}y^2 \times\left(2r_{\rm TM} - \frac{4a^2\alpha_{\rm FS}^2\xi^2}{y^2}(r_{\rm TM}+r_{\rm TE})\right) \tag{2}$$

and

$$C_3(a,T) = -\frac{k_BT}{8}{\sum_l}'\alpha(\iota\zeta_l\omega_c)\int_{\zeta_l}^\infty dy\{e^{-y}2y^2\zeta_l{}^2 r_{\rm TM}(\iota\zeta_l,y) \times[r_{\rm TM}(\iota\zeta_l,y)+r_{\rm TE}(\iota\zeta_l,y)]\}, \tag{3}$$

respectively, where $\alpha_{\rm FS}$ is the fine-structure constant and $\alpha(\iota\omega)$ is the dynamic polarizability of the respective atomic system along the imaginary frequency $\iota\omega$. In the above expressions, it is assumed that graphene is in thermal equilibrium at temperature T. It is obvious from the above expressions that an accurate estimate of C_3 coefficients requires accurate values of the dynamic polarizabilities $\alpha(\iota\xi_l)$ along the imaginary Matsubara frequencies $\xi_l = 2\pi k_BTl/\hbar$ with $l = 0,1,2,\ldots$ of the considered atomic systems. It should also be noted that the prime over the summation sign in the above expression indicates multiplication of the $l = 0$ term by a factor of $1/2$. The reflection coefficients of the electromagnetic oscillations on graphene in the Dirac model defined at nonzero temperature are given by [14,43]

$$r_{\rm TM}(\iota\zeta_l,y) = \frac{y\tilde{\Pi}_{00}}{y\tilde{\Pi}_{00}+2\left(y^2-\zeta_l^2\right)} \tag{4}$$

and

$$r_{\rm TE}(\iota\zeta_l,y) = -\frac{\left(y^2-\zeta_l^2\right)\tilde{\Pi}_{\rm tr}-y^2\tilde{\Pi}_{00}}{\left(y^2-\zeta_l^2\right)(\tilde{\Pi}_{\rm tr}+2y)-y^2\tilde{\Pi}_{00}}, \tag{5}$$

where $\tilde{\Pi}_{00}$ and $\tilde{\Pi}_{\rm tr}$ are the components of dimensionless polarization tensors given in [14,43]. The above expressions include a certain physical quantity Δ, known as the gap parameter. This parameter is adjusted to instigate the atom-graphene interaction coefficient. Although the exact value of Δ is unknown, its maximum value is assumed to be 0.1 eV. However, we take $\Delta = 0.01$ eV throughout the paper.

Recently, a different representation for the polarization tensor was derived by Bordag *et al.* [44]. They showed that the previously used polarization tensor of Ref. [43] is correct only at the imaginary Matsubara frequencies, but it cannot propagate continuously from the complex frequency plane to the real frequency axis. Nevertheless, it was also shown that this representation for the polarization tensor allows one to estimate the reflection coefficients approximately at the Matsubara frequencies, which considerably simplifies evaluation of the interaction potential due to the van der Waals forces in graphene systems [45]. In the present work, however, we take into account the reflection coefficients at zero and nonzero temperatures from the previous studies [14,39,43] and give more emphasis on the use of precise values of the dynamic polarizabilities in the determination of the C_3 coefficients to describe the interactions of the considered atomic systems with a graphene layer. In the following section we discuss briefly the approaches adopted to evaluate these polarizabilities.

III. APPROACHES TO EVALUATE POLARIZABILITIES

The expression for the dynamic dipole polarizability of an atomic state $|\Psi_0^{(0)}\rangle$ with an imaginary frequency $\iota\omega$ is given by

$$\alpha(\iota\omega) = -2\frac{\langle\Psi_0^{(0)}|D|\Psi_0^{(1)}\rangle}{\langle\Psi_0^{(0)}|\Psi_0^{(0)}\rangle}, \tag{6}$$

where $|\Psi_0^{(1)}\rangle$ is the first-order perturbed wave function to $|\Psi_0^{(0)}\rangle$ due to the dipole operator D and the solution of the first-order differential equation

$$\left(H-E_0^{(0)}-\iota\omega\right)|\Psi_0^{(1)}\rangle = \frac{(E_0-H)D}{H-E_0+\iota\omega}|\Psi_0^{(0)}\rangle \tag{7}$$

for the atomic Hamiltonian H, which is taken in the Dirac-Coulomb approximation for the present work, and $E_0^{(0)}$ is the energy eigenvalue corresponding to the state $|\Psi_0^{(0)}\rangle$. In the above expression, difficulties with the accurate estimate of α lie in the determination of both $|\Psi_0^{(0)}\rangle$ and $|\Psi_0^{(1)}\rangle$ of an atomic system. One can also write the above expression in the sum-over-states approach as

$$\alpha(\iota\omega) = -\frac{2}{\langle\Psi_0^{(0)}|\Psi_0^{(0)}\rangle}\sum_{I\neq0}\frac{\left(E_0^{(0)}-E_I^{(0)}\right)\left|\langle\Psi_0^{(0)}|D|\Psi_I^{(0)}\rangle\right|^2}{E_0^{(0)}-E_I^{(0)}+\omega^2}, \tag{8}$$

where I represents all possible allowed intermediate states with their corresponding energies $E_I^{(0)}$. This approach can be conveniently employed to one-valence atomic systems such as the alkali-metal atoms and singly charged alkaline-earth-metal ions to determine their polarizabilities as the matrix elements $\langle\Psi_0^{(0)}|D|\Psi_I^{(0)}\rangle$ among large intermediate states of these systems can be calculated using the Fock-space relativistic coupled-cluster (RCC) method, as has been demonstrated elaborately in our previous work [46], and the excitation energies can be taken from the measurements. We use the polarizabilities of the alkaline-earth-metal ions that were given in our previous work [46], but the polarizabilities for the alkali-metal ions and inert-noble-gas atoms are obtained using the following procedure.

It is not advisable to employ the sum-over-states approach to determine the polarizabilities of the atomic systems having inert-gas atomic configurations as an evaluation of the dipole ($E1$) matrix elements of the dipole operator among different intermediate states of these systems is extremely difficult and might require us to employ an approach similar to the equation-of-motion-based many-body theory for their evaluation. This will demand large computational resources and sometime it may not be possible to calculate the $E1$ matrix elements for a sufficiently large number of intermediate states to estimate the polarizabilities within the required accuracies. One of the other appropriate approaches to determine polarizabilities of these inert-gas atomic systems within the RCC method framework was demonstrated in [50,70,71]. Use of these RCC methods is also time consuming and can demand large computational resources. Since the addressed problem requires dynamic polarizabilities for a large set of imaginary frequencies, employing the above-mentioned RCC method is impractical within a stimulated time frame to analyze the dispersion coefficients for all the considered inert-gas atoms. Moreover, the above methods are appropriate only for calculating scalar polarizabilities and dynamic polarizabilities with real frequency arguments after a slight modification in the methodology (details are irrelevant to describe here). However, it cannot be applied adequately to determine dynamic polarizabilities with imaginary frequency arguments. It has been demonstrated in earlier studies [50,70,71] that scalar polarizabilities of the inert-gas atomic systems evaluated using the relativistic random-phase approximation (RPA) match reasonably well with their experimental values. Thus, consideration of the RPA can be good enough to determine dynamic polarizabilities of the inert-gas atomic systems. The advantage of applying this method is twofold: First, calculation of polarizability for a given frequency can be performed within a reasonable time frame and second, a slightly modified RPA can be employed to determine dynamic polarizabilities at the imaginary frequencies as demonstrated below. In the RPA, the expression for the dipole polarizability is given by

$$\alpha(\iota\omega) = 2\langle\Phi_0|D\big|\Psi^{(1)}_{\rm RPA}\big\rangle. \tag{9}$$

This clearly suggests that the wave function $|\Psi^{(0)}_0\rangle$ in Eq. (6) is approximated to $|\Phi_0\rangle$, which is nothing but a mean-field wave function and is obtained using the Dirac-Fock method in this work, and the first-order perturbed wave function is given by $|\Psi^{(1)}_{\rm RPA}\rangle$. In the RPA framework, we obtain $|\Psi^{(1)}_{\rm RPA}\rangle$ as

$$\begin{aligned}\big|\Psi^{(1)}_{\rm RPA}\big\rangle &= \sum_{\beta}^{\infty}\sum_{p,a}\Omega^{(\beta,1)}_{a\to p}|\Phi_0\rangle \\ &= \sum_{\beta=1}^{\infty}\sum_{pq,ab}\left(\frac{[\langle pb|(1/r_{12})|aq\rangle - \langle pb|(1/r_{12})|qa\rangle]\Omega^{(\beta-1,1)}_{b\to q}}{(\epsilon_p-\epsilon_a)^2+\omega^2} + \frac{\Omega^{(\beta-1,1)^\dagger}_{b\to q}[\langle pq|(1/r_{12})|ab\rangle - \langle pq|(1/r_{12})|ba\rangle]}{(\epsilon_p-\epsilon_a)^2+\omega^2}\right) \\ &\quad\times(\epsilon_p-\epsilon_a)|\Phi_0\rangle,\end{aligned} \tag{10}$$

where $\Omega^{(\beta,1)}_{a\to p}$ is a wave operator that excites an occupied orbital a of $|\Phi_0\rangle$ to a virtual orbital p that alternatively refers to a singly excited state with respect to $|\Phi_0\rangle$ with $\Omega^{(0,1)}_{a\to p} = \frac{\langle p|(\epsilon_p-\epsilon_a)D|a\rangle}{(\epsilon_p-\epsilon_a)^2+\omega^2}$ for the single-particle orbitals energies ϵ and the superscripts β and 1 represent the number of Coulomb ($\frac{1}{r_{12}}$ in atomic units) and D operators, respectively.

IV. RESULTS AND DISCUSSION

We present the scalar polarizability $\alpha(0)$ values for all the considered atomic systems in Table I obtained using our calculations and compare them against the results available from other theoretical studies using a variety of many-body methods and experimental measurements. Among the other theoretical works, Johnson *et al.* [47] have performed the RPA calculations for the singly ionized alkali-metal ions; our results are found to be consistent with their values. In another work, Soldan *et al.* [67] reported these values by employing the coupled-cluster method. Lim *et al.* [51] have also evaluated these polarizabilities by employing the RCC method and considering the scalar relativistic atomic Hamiltonian, but their values are found to be larger than the RPA and experimental results. The reason could be that their approximated method may be overestimating the correlation effects beyond the RPA contributions. Nakajima and Hirao [69] also investigated the polarizability values for inert-gas systems using the relativistic effects in the estimate of α using the Douglas-Kroll Hamiltonian and adopting the finite gradient method. Sahoo and co-workers report these values for many systems using the RCC method [50,57,60]. The calculations by Patil and Tang [59] were carried out by using multipole matrix elements calculated from simple wave functions based on the asymptotic behavior and the binding energies of the valence electron. Safronova *et al.* [64] calculated the polarizabilities using the relativistic all-order single-double method where all the single and double excitations of the Dirac-Fock wave function are included to all orders of perturbation theory. For the Li^+ ion, Cooke *et al.* [49] determined the dipole polarizability from the *d-f* and *d-g* energy splittings using a laser excitation and optical detection scheme. The dipole polarizabilities of closed-shell Na^+ and K^+ ions are obtained from observed spectra, using theoretical values of quadrupole polarizabilities taken from the literature and including a number of corrections up to the fourth order in Ref. [52]. Our results for Rb^+ ion are in close agreement with the experimental values given by Johansson [53]. Experimental analysis of the dipole polarizability values for the Ca^+ ion has been done by Chang [56]. However,

TABLE I. Comparison of the scalar polarizabilities $\alpha(0)$ of the alkali-metal ions (Li^+, Na^+, K^+, and Rb^+), alkaline-earth-metal ions (Ca^+, Sr^+, Ba^+, and Ra^+), and inert-gas atoms (He, Ne, Ar, and Kr) from different theoretical and experimental works. References are given inside square brackets.

System	This work	Other works	Experiment
Li^+	0.19	0.1894 [47], 0.192486 [48] 0.1913 [50]	0.188 [49]
Na^+	0.95	0.9457 [47], 1.00 [51] 0.9984 [50]	0.978 [52]
K^+	5.45	5.457 [47], 5.52 [51] 5.522 [50]	5.47 [52]
Rb^+	9.06	9.076 [47], 9.11 [51] 9.213 [50]	9.0 [53]
Ca^+	76.77	75.88 [54], 75.49 [55] 73.0 [57], 76.1 [58], 75.5 [59]	75.3 [56]
Sr^+	92.24	88.29 [60], 91.10 [54] 91.3 [62], 91.47 [59]	93.3 [61]
Ba^+	124.40	124.26 [60], 123.07 [54] 124.7 [59]	123.88 [63]
Ra^+	105.91	105.37 [54], 106.5 [64] 104.54 [60], 106.12 [65] 106.22 [66]	
He	1.32	1.32 [47], 1.383 [67] 1.360 [50]	1.3838[68]
Ne	2.37	2.38 [47], 2.697 [69] 2.652 [50]	2.668 [68]
Ar	10.77	10.77 [47], 11.22 [69] 11.089 [50]	11.091 [68]
Kr	16.47	16.47 [47], 16.8 [69] 16.93 [50]	16.74 [68]

the ground-state polarizability of the Sr^+ ion given in [61] by Barklem and O'Mara using oscillator strength sum rules has a considerable discrepancy with our results. Snow and Lundeen [63] have performed high-precision measurements for calculating polarizability of Ba^+ ion using a different technique based on the resonant Stark ionization spectroscopy microwave technique. We observe that our results are in agreement with the experimental values. There is a noticeable variance in the polarizabilities of inert atoms Ne and Ar from the experimental results [68] by Langhoff and Karplus; they employed a method based on the Cauchy dispersion equation and Padé approximates are used for extrapolation, which improves the convergence of the Cauchy equation.

A comparison between these results shows that our methods give reasonably accurate $\alpha(0)$ values, thus these methods can be employed to determine dynamic polarizabilities in these atomic systems within accuracies similar to that observed in the evaluation of the scalar polarizabilities. We plot these dynamic polarizabilities in Figs. 1 and 2, which show that alkaline-earth-metal ions have the highest polarizabilities, followed by inert-gas atoms and then alkali-metal ions.

Using the dynamic polarizabilities given above, we now determine the dispersion coefficients of the considered alkali-metal ions, alkaline-earth-metal ions, and inert-gas atoms interacting with a graphene layer with the reflection coefficients estimated using the Dirac model. This is an extension of our previous work [15], where the interaction of the alkali-metal atoms with a graphene layer was investigated. Here we adopt the approaches described in Refs. [14,16] to evaluate the reflection coefficients for the determination of C_3 coefficients as a function of separation distance of an atomic system from the graphene layer and a function of temperature. These results are discussed systematically below for each class of atomic system.

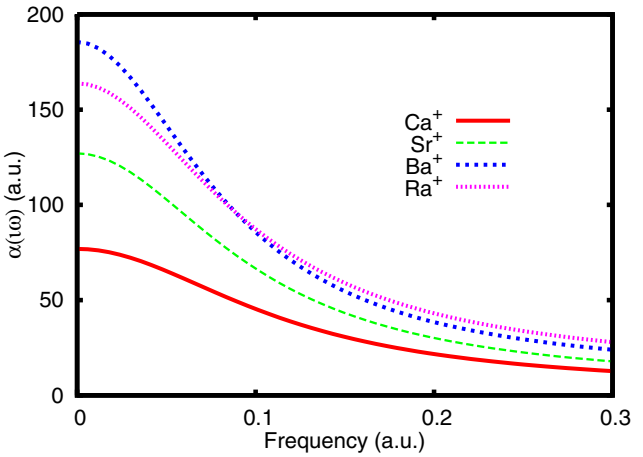

FIG. 1. (Color online) Dynamic polarizabilities of the alkaline-earth-metal ions Ca^+, Sr^+, Ba^+, and Ra^+ interacting with a graphene layer as functions of frequency.

A. Interactions of alkali-metal ions with a graphene layer

In Fig. 3, the graph between C_3 coefficients as a function of the separation distance a (in nm) for the interactions of alkali-metal ions Li^+, Na^+, K^+, and Rb^+ with a graphene layer is shown for a gap parameter $\Delta = 0.01$ eV. The solid red curve corresponds to room temperature $T = 300$ K, while the dashed green curve represents the $T = 0$ K temperature of the C_3 coefficients. It should be noted that the reflection coefficients being same for a particular interacting surface (in our case, graphene), at a specific separation distance and temperature,

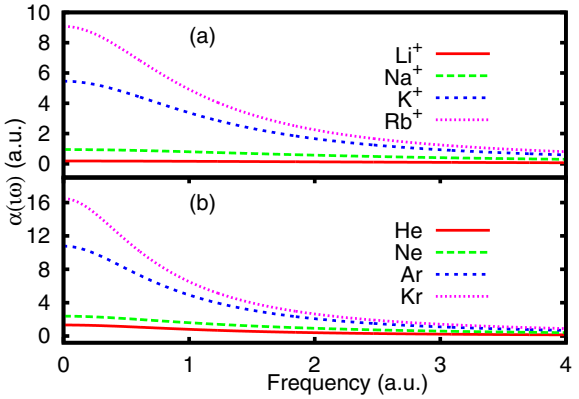

FIG. 2. (Color online) Dynamic polarizabilities of the (a) alkali-metal ions Li^+, Na^+, K^+, and Rb^+ and (b) inert-gas atoms He, Ne, Ar, and Kr interacting with a graphene layer as functions of frequency.

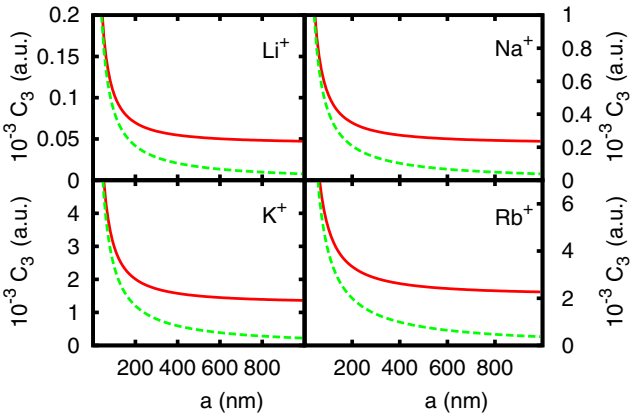

FIG. 3. (Color online) The C_3 coefficients (in a.u.) as a function of the ion-graphene separation distance for the alkali-metal ions Li^+, Na^+, K^+, and Rb^+ interacting at $T = 300$ K (solid red curve) and $T = 0$ K (dashed green curve).

the C_3 coefficients of an element completely depend on its dynamic dipole polarizabilities. It was found in [16] that the C_3 coefficients increase with a corresponding increase in the atomic sizes of the alkali-metal atoms for a given separation distance. In the same manner, it can be seen that there is a likewise increase in the dispersion C_3 coefficients with an increase in the size of alkali-metal ions at a particular distance of separation. It can also be observed from this figure that the interaction between these ions and a graphene layer is more effective at short separations while it is negligible at large separation distances.

B. Interactions of alkaline-earth-metal ions with graphene

The dispersion interactions of the alkaline-earth-metal ions Ca^+, Sr^+, Ba^+, and Ra^+ with a graphene layer at temperatures $T = 300$ K (solid red curve) and $T = 0$ K (dashed green curve) are shown in Fig. 4. It can be clearly seen from this figure that these C_3 coefficients are large for comparatively large ions except for the Ba^+ ion. This dominance of the Ba^+ ion C_3 coefficient over the Ra^+ ion coefficient is due to the fact that the polarizability of Ba^+ ion is larger than that of Ra^+ [46,64,71]. The reduction in the polarizability of the Ra^+ ion is owing to the dominant contribution of the relativistic effects over the correlation effects [54]. Again, it can be seen in the figure that the interaction between these ions with a graphene layer is more effective at short separations and becomes insignificant at large separation distances. Of the three types of atomic systems, the interaction of graphene with alkaline-earth ions is the strongest one. For a separation distance of 300 nm, the interaction of alkaline-earth-metal ions with graphene layer is approximately 14 times stronger than the interaction with alkali-metal ions and approximately 8 times stronger than the interaction with inert-gas atoms. At the same time, one should keep in mind that graphene is a conductor. Simple estimation using the method of electrostatic images shows that the electric force between an ion and a graphene layer is much stronger than the Casimir-Polder force even at the shortest possible separation distance. Because of this, the Casimir-Polder force does not play an important role in the interaction of ions with the surface of graphene.

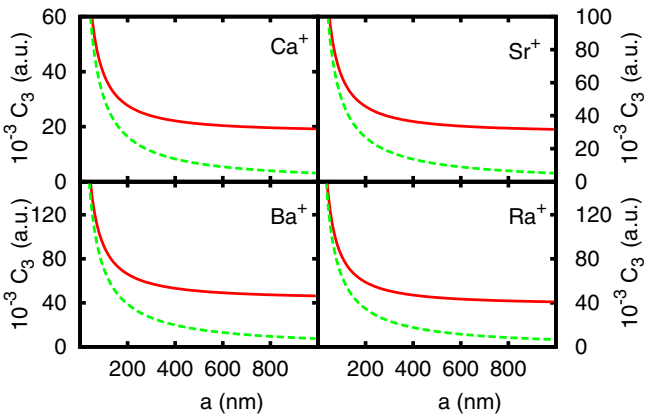

FIG. 4. (Color online) The C_3 coefficients (in a.u.) calculated for the interactions of the alkaline-earth-metal ions Ca^+, Sr^+, Ba^+, and Ra^+ with a graphene layer as a function of separation distance a (in nm) at temperatures $T = 300$ K (red solid curve) and $T = 0$ K (green dashed curve).

C. Interactions of inert-gas atoms with graphene

The graph for the interactions between the inert-gas atoms with a graphene layer, as a function of separation distance a, is presented in Fig. 5. We can clearly observe from the figure that C_3 coefficients of the ion-graphene interactions are large for comparatively large ions, owing to their greater values of scalar polarizability. These coefficients are shown for temperatures $T = 300$ K (solid red curve) and $T = 0$ K (dashed green curve). It can be seen from Fig. 5 that the dispersion coefficients calculated at room temperature show much less variation from the zero-temperature coefficients at small separations, whereas at the larger distances of separation we find comparatively stronger dispersion interactions at $T = 300$ K than at $T = 0$ K.

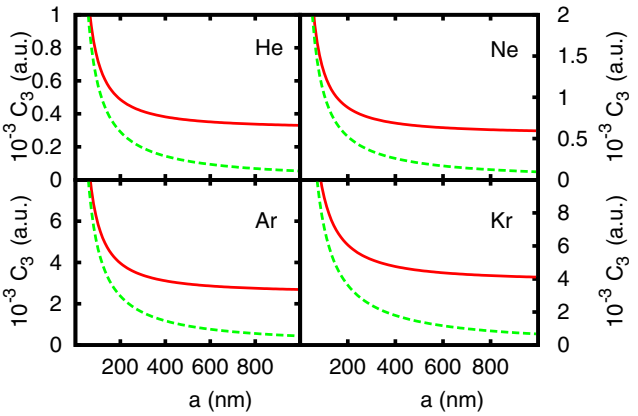

FIG. 5. (Color online) The C_3 coefficients (in a.u.) for the interactions of the inert-gas atoms He, Ne, Ar, and Kr with graphene as a function of the separation distance a (in nm) at temperatures $T = 300$ K (solid red curve) and $T = 0$ K (dashed green curve).

TABLE II. Fitting parameters for the C_3 (a and $T = 300$ K) coefficients of the considered alkali-metal ions, alkaline-earth-metal ions, and inert-gas atoms with a graphene layer. Here A_1 and A_2 are given on the order of 10^{-2} a.u. and x_0 in nm.

	Alkali-metal ions			
Parameters	Li^+	Na^+	K^+	Rb^+
A_1	0.48798	2.41443	13.3224	21.6418
A_2	0.00368	0.01841	0.10702	0.17863
x_0	1.5239	1.53425	1.58631	1.61405
	Alkaline-earth-metal ions			
Parameters	Ca^+	Sr^+	Ba^+	Ra^+
A_1	66.8551	100.604	136.182	137.158
A_2	1.71017	2.84881	4.19032	3.66618
x_0	3.28993	3.49327	3.64421	3.31959
	Inert-gas atoms			
Parameters	He	Ne	Ar	Kr
A_1	3.214	5.8524	24.7463	36.6345
A_2	0.02594	0.04662	0.2133	0.32761
x_0	1.59107	1.57743	1.65885	1.69824

D. Fitting formula

In contemplation of simplification in generating our results of C_3 coefficients for future theoretical and experimental verifications or for extracting these values for various applications at room temperature with a given separation distance, we provide a logistic fit of the functional form of these coefficients as

$$C_3(a) = A_2 + \frac{A_1 - A_2}{1 + a/x_0}, \tag{11}$$

where A_1 (in a.u.), A_2 (in a.u.), and x_0 (in nm) are the fitting parameters that rely on the properties of the interacting atomic systems with a graphene layer. We give our fitting coefficients in Table II for extrapolating the dispersion coefficients for the considered element–graphene layer interactions. We predict that the coefficients obtained using the above fitting parameters have divergences not more than 6% with the coefficients calculated using the Dirac model at $T = 300$ K. Hence, the above equation serves as the best suited fit to express the interactions of the considered atomic systems with a graphene layer.

V. CONCLUSION

We have studied the dispersion interaction coefficients of the alkali-metal ions (Li^+, Na^+, K^+, and Rb^+), alkaline-earth-metal ions (Ca^+, Sr^+, Ba^+, and Ra^+), and inert-gas atoms (He, Ne, Ar, and Kr) with a graphene layer. We have shown explicitly the dependence of these coefficients on the separation distance a and temperature T. We commenced by using accurate values of the dynamic polarizabilities of the considered atomic systems by employing suitable relativistic many-body methods and calculating the reflection coefficients using the Dirac model. We observed that the dispersion interaction coefficients of the alkaline-earth-metal ions with the graphene layer is the strongest among the alkali-metal ions and inert-gas atoms interacting with graphene; the weakest dispersion interaction of graphene is with the alkali-metal ions. It is also seen that due to the larger values of dynamic polarizabilities of the Ba^+ ion than those of the Ra^+ ion, the dispersion coefficient of Ba^+ dominates over the Ra^+ ion. Although the Casimir-Polder force between ions and the graphene surface is negligibly small compared to the electric force, our results for inert-gas atoms can be of great use for experimentalists in studying these interactions more reliably in view of the fact that performing these experiments at room temperature is comparatively more susceptible. This study also demonstrates the stronger dispersion interactions of the alkaline-earth-metal ions, especially at larger distances of separations, and its results can be widely applied. In addition, we also devise a promptly accessible functional form of logistic type having a separation distance dependence at room temperature for easy extraction of the dispersion coefficients for future applications.

ACKNOWLEDGMENTS

The work of B.A. was supported by CSIR Grant No. 03(1268)/13/EMR-II, India. K.K. acknowledges financial support from DST (Grant No. DST/INSPIRE Fellowship/2013/758). B.K.S. acknowledges use of the PRL 3TFlop HPC cluster at Ahmedabad.

[1] K. S. Novoselov, A. K. Geim, S. V. Morozov, D. Jiang, Y. Zhang, S. V. Dubonos, I. V. Grigorieva, and A. A. Firsov, Science **306**, 666 (2004).
[2] A. K. Geim and K. S. Novoselov, Nat. Mater. **6**, 183 (2007).
[3] H. Friedrich, G. Jacoby, and C. G. Meister, Phys. Rev. A **65**, 032902 (2002).
[4] S. Iijima, Nature (London) **354**, 56 (1991).
[5] T. W. Ebbesen and P. M. Ajayan, Nature (London) **358**, 220 (1992).
[6] T. Guo, P. Nikolaev, A. G. Rinzler, D. Tomanek, D. T. Colbert, and R. E. Smalley, J. Phys. Chem. **99**, 10694 (1995).
[7] D. J. Mowbray, Z. L. Miskovic, and F. O. Goodman, Phys. Rev. B **74**, 195435 (2006).
[8] K. S. Novoselov, V. I. Fal'ko, L. Colombo, P. R. Gellert, M. G. Schwab, and K. Kim, Nature (London) **490**, 192 (2012).
[9] Q. Zhang, S. Wu, L. Zhang, J. Lu, F. Verproot, Y. Liu, Z. Xing, J. Li, and X. M. Song, Biosens. Bioelectron **26**, 2632 (2011).
[10] Y. Chan and J. M. Hill, Micro Nano Lett. **5**, 247 (2010).
[11] T. A. Hilder and J. M. Hill, Curr. Appl. Phys. **8**, 258 (2007).
[12] S. Tang and Z. Cao, J. Chem. Phys. **134**, 044710 (2011).
[13] Y. Wang, Y. Shao, D. W. Matsun, J. Li, and Y. Lin, ACS Nano **4**, 1790 (2010).
[14] M. Chaichian, G. L. Klimchitskaya, V. M. Mostepanenko, and A. Tureanu, Phys. Rev. A **86**, 012515 (2012).
[15] K. Kaur, J. Kaur, B. Arora, and B. K. Sahoo, Phys. Rev. B **90**, 245405 (2014).

[16] B. Arora, H. Kaur, and B. K. Sahoo, J. Phys. B **47**, 155002 (2014).
[17] W. A. Diño, H. Nakanishi, H. Kasai, T. Sugimoto, and T. Kondo, e-J. Surf. Sci. Nanotechnol. **2**, 77 (2004).
[18] A. Bogicevic, S. Ovesson, P. Hyldgaard, B. I. Lundqvist, H. Brune, and D. R. Jennison, Phys. Rev. Lett. **85**, 1910 (2000).
[19] J. Jung, P. Garcia-Gonzalez, J. F. Dobson, and R. W. Godby, Phys. Rev. B **70**, 205107 (2004).
[20] J. F. Dobson, A. White, and A. Rubio, Phys. Rev. Lett. **96**, 073201 (2006).
[21] E. Hult, P. Hyldgaard, J. Rossmeisl, and B. I. Lundqvist, Phys. Rev. B **64**, 195414 (2001).
[22] I. V. Bondarev and P. Lambin, Phys. Rev. B **70**, 035407 (2004).
[23] A. O. Caride, G. L. Klimchitskaya, V. M. Mostepanenko, and S. I. Zanette, Phys. Rev. A **71**, 042901 (2005).
[24] E. V. Blagov, G. L. Klimchitskaya, and V. M. Mostepanenko, Phys. Rev. B **71**, 235401 (2005).
[25] J. F. Babb, G. L. Klimchitskaya, and V. M. Mostepanenko, Phys. Rev. A **70**, 042901 (2004).
[26] M. Bordag, G. L. Klimchitskaya, and V. M. Mostepanenko, Phys. Rev. B **86**, 165429 (2012).
[27] D. Jiang and S. D. M. H. Du, J. Chem. Phys. **130**, 074705 (2009).
[28] J. Wintterlin and M. L. Bocquet, Surf. Sci. **603**, 1841 (2009).
[29] Y. V. Churkin, A. B. Fedortsov, G. L. Klimchitskaya, and V. A. Yurova, Phys. Rev. B **82**, 165433 (2010).
[30] M. S. Dresselhaus and G. Dresselhaus, Adv. Phys. **51**, 1 (2002).
[31] C. K. Yang, Appl. Phys. Lett. **94**, 163115 (2009).
[32] X.-k. Konga and Q.-w. Chen, Phys. Chem. Chem. Phys. **15**, 12982 (2013).
[33] J. W. Burress, S. Gadipelli, J. Ford, J. M. Simmons, W. Zhou, and T. Yildirim, Angew. Chem. Int. **49**, 8902 (2010).
[34] V. Tozzini and V. Pellegrini, Phys. Chem. Chem. Phys. **15**, 80 (2013).
[35] K. Spyrou, D. Gournis, and P. Rudolf, ECS J. Solid State Sci. Technol. **2**, M3160 (2013).
[36] M. Bordag, U. Mohideen, and V. M. Mostepanenko, Phys. Rep. **353**, 1 (2001).
[37] M. Bordag, B. Geyer, G. L. Klimchitskaya, and V. M. Mostepanenko, Phys. Rev. B **74**, 205431 (2006).
[38] E. V. Blagov, G. L. Klimchitskaya, and V. M. Mostepanenko, Phys. Rev. B **75**, 235413 (2007).
[39] M. Bordag, I. V. Fialkovsky, D. M. Gitman, and D. V. Vassilevich, Phys. Rev. B **80**, 245406 (2009).
[40] Y. V. Churkin, A. B. Fedortsov, G. L. Klimchitskaya, and V. A. Yurova, Int. J. Mod. Phys.: Conf. Ser. **3**, 555 (2011).
[41] G. L. Klimchitskaya and V. M. Mostepanenko, Phys. Rev. B **91**, 045412 (2015).
[42] M. Bordag, G. Klimchitskaya, U. Mohideen, and V. M. Mostepanenko, *Advances in the Casimir Effect* (Oxford University Press, Oxford, 2009).
[43] I. V. Fialkovsky, V. N. Marachevsky, and D. V. Vassilevich, Phys. Rev. B **84**, 035446 (2011).
[44] M. Bordag, G. L. Klimchitskaya, V. M. Mostepanenko, and V. M. Petrov, Phys. Rev. D **91**, 045037 (2015).
[45] G. L. Klimchitskaya and V. M. Mostepanenko, Phys. Rev. B **91**, 174501 (2015).
[46] J. Kaur, D. K. Nandy, B. Arora, and B. K. Sahoo, Phys. Rev. A **91**, 012705 (2015).
[47] W. R. Johnson, D. Kolb, and K. Huang, At. Data Nucl. Data Tables **28**, 333 (1983).
[48] A. K. Bhatia and R. J. Drachman, Can. J. Phys. **75**, 11 (1997).
[49] W. E. Cooke, T. F. Gallagher, R. M. Hill, and S. A. Edelstein, Phys. Rev. A **16**, 1141 (1977).
[50] Y. Singh, B. K. Sahoo, and B. P. Das, Phys. Rev. A **88**, 062504 (2013).
[51] I. S. Lim, J. K. Laerdahl, and P. Schwerdtfeger, J. Chem. Phys. **116**, 172 (2002).
[52] U. Opik, Phys. Soc. **92**, 566 (1967).
[53] I. Johansson, Ark. Fys. **20**, 135 (1961).
[54] I. S. Lim and P. Schwerdtfeger, Phys. Rev. A **70**, 062501 (2004).
[55] J. Mitroy and J. Y. Zhang, Eur. Phys. J. D **46**, 415 (2008).
[56] E. S. Chang, J. Phys. B **16**, L539 (1983).
[57] B. K. Sahoo, B. P. Das, and D. Mukherjee, Phys. Rev. A **79**, 052511 (2009).
[58] B. Arora, M. S. Safronova, and C. W. Clark, Phys. Rev. A **76**, 064501 (2007).
[59] S. H. Patil and K. T. Tang, J. Chem. Phys. **106**, 2298 (1997).
[60] B. K. Sahoo, R. G. E. Timmermans, B. P. Das, and D. Mukherjee, Phys. Rev. A **80**, 062506 (2009).
[61] P. S. Barklem and B. J. O'Mara, Mon. Not. R. Astron. Soc. **311**, 535 (2000).
[62] D. Jiang, B. Arora, M. S. Safronova, and C. W. Clark, J. Phys. B **42**, 154020 (2009).
[63] E. L. Snow and S. R. Lundeen, Phys. Rev. A **76**, 052505 (2007).
[64] U. I. Safronova, W. R. Johnson, and M. S. Safronova, Phys. Rev. A **76**, 042504 (2007).
[65] B. K. Sahoo, B. P. Das, R. K. Chaudhuri, D. Mukherjee, R. G. E. Timmermans, and K. Jungmann, Phys. Rev. A **76**, 040504(R) (2007).
[66] R. Pal, D. Jiang, M. S. Safronova, and U. I. Safronova, Phys. Rev. A **79**, 062505 (2009).
[67] P. Soldan, E. P. F. Lee, and T. G. Wright, Phys. Chem. **3**, 4661 (2001).
[68] P. W. Langhoff and M. Karplus, J. Opt. Soc. Am. **59**, 863 (1969).
[69] T. Nakajima and K. Hirao, Chem. Lett. **30**, 766 (2001).
[70] Y. Singh, B. K. Sahoo, and B. P. Das, Phys. Rev. A **89**, 030502(R) (2014); **90**, 039903(E) (2014).
[71] B. K. Sahoo and B. P. Das, Phys. Rev. A **77**, 062516 (2008).